

U U U J 4 2 U 6 7 2 7

To be presented at the Symposium on  
Micromechanical Modeling of Flow and  
Fracture, Rensselaer Polytechnic  
Institute, Troy, New York, June 23-25,  
1975; Submitted to Journal of Engineering  
Materials and Technology

LBL-3508  
Preprint c.1

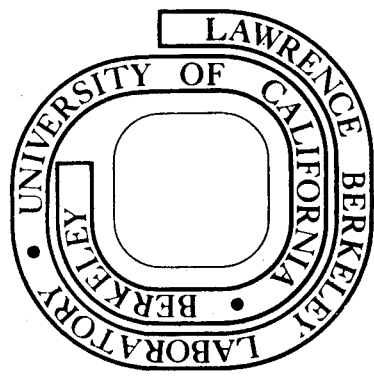
COMPUTER SIMULATION OF PLASTIC DEFORMATION THROUGH  
PLANAR GLIDE IN AN IDEALIZED CRYSTAL

Sabri Altintas, Kenton Hanson and J. W. Morris, Jr.

October, 1974

Prepared for the U. S. Atomic Energy Commission  
under Contract W-7405-ENG-48

**For Reference**  
Not to be taken from this room



LBL-3508  
c.1

## **DISCLAIMER**

This document was prepared as an account of work sponsored by the United States Government. While this document is believed to contain correct information, neither the United States Government nor any agency thereof, nor the Regents of the University of California, nor any of their employees, makes any warranty, express or implied, or assumes any legal responsibility for the accuracy, completeness, or usefulness of any information, apparatus, product, or process disclosed, or represents that its use would not infringe privately owned rights. Reference herein to any specific commercial product, process, or service by its trade name, trademark, manufacturer, or otherwise, does not necessarily constitute or imply its endorsement, recommendation, or favoring by the United States Government or any agency thereof, or the Regents of the University of California. The views and opinions of authors expressed herein do not necessarily state or reflect those of the United States Government or any agency thereof or the Regents of the University of California.

COMPUTER SIMULATION OF PLASTIC DEFORMATION  
THROUGH PLANAR GLIDE IN AN IDEALIZED CRYSTAL

by

Sabri Altintas, Kenton Hanson, and J. W. Morris, Jr.

Inorganic Materials Research Division, Lawrence Berkeley Laboratory and  
Department of Materials Science and Engineering, College of Engineering  
University of California, Berkeley, California 94720

ABSTRACT

In this paper we report the behavior of the plastic deformation of an idealized crystal made by stacking parallel slip planes. Each slip plane is assumed to contain active sources of dislocations leading to a constant density of non-interacting dislocations in the plane which glide through randomly distributed localized point obstacles, representing small precipitates. The dislocation is assumed to have a constant line tension and the dislocation-obstacle interaction is taken to have a simple step form.

Using results of computer simulation of thermally activated glide through random arrays of point obstacles we modelled deformation as a function of temperature and applied stress, determining the strain rate and the morphological characteristics of slip.

## I. INTRODUCTION

The plastic deformation of a typical crystal is accomplished through the motion of dislocations. At moderate temperature the dominant form of dislocation motion is planar glide, which is impelled by the local value of the resolved shear stress and opposed by the resistance of the microstructure. The dominant impediment to glide is often due to local microstructural features such as small precipitates, "forest" dislocations, or solute atoms which act as local barriers to dislocation motion.<sup>(1)</sup> When these are spread diffusely through the lattice they may often be regarded as point barriers in an approximately random distribution.

Under suitable idealizations the problem of thermally activated dislocation glide through a field of point barriers can be simulated on a computer for direct solution.<sup>(2-4)</sup> In previous papers<sup>(4-6)</sup> we have discussed how statistical analysis and computer simulation may be combined to yield an essentially complete solution for the velocity of dislocation glide as a function of the applied stress, the temperature, and the nature of the barriers. By adding an assumption on the distribution of mobile dislocations, the results may be extended to model deformation of a single crystal which is assumed to deform through simultaneous glide of non-interacting dislocations on adjacent slip planes.

In Reference 4 we reported preliminary results of a simulation of the deformation of a simple crystal at constant strain rate. The results were interesting in that the crystal not only showed the anticipated trend of flow stress with temperature but also exhibited a characteristic shift in the morphology of deformation with temperature: low temperature

deformation concentrated on well-defined slip planes which became less pronounced as the temperature was raised.

To continue exploration of this behavior we simulated the plastic deformation of an ideal crystal made up of a stacking of slip planes containing randomly dispersed obstacles having roughly the properties expected of small dispersion or precipitate particles. Each slip plane was assumed to contain active sources of dislocations leading to a constant density of non-interacting dislocations in the plane. We then modelled deformation as a function of temperature and applied stress, determining the strain rate and the morphological characteristics of slip. The results are reported below. We first review the basic equations governing thermally activated glide and describe the simulation procedure.

## II. BASIC EQUATIONS

The assumptions and basic equations governing thermally activated glide of a simple dislocation through a field of randomly-distributed point barriers were developed in detail in Reference 5. They may be summarized as follows:

Consider a crystal plane which is the glide plane of a dislocation. Let it contain a random distribution of microstructural barriers which are represented<sup>(7)</sup> as point obstacles to dislocation glide. The array is described by the statement that its points are randomly distributed and by a characteristic length

$$l_s = a^{1/2}$$

(1)

where  $a$  is the mean area per point. A dislocation in this plane is modelled as a flexible, extensible string having a constant line tension,  $\Gamma$ , and a Burgers' vector of magnitude  $b$ , taken to lie in the plane. The resolved shear stress,  $\tau$ , impelling glide of this dislocation may be conveniently written in dimensionless form

$$\tau^* = \tau l_s b / 2\Gamma \quad (2)$$

Let the dislocation be pressed against a configuration of point obstacles (denoted by  $i$ ) by the applied stress  $\tau^*$  (Figure 1). Between two adjacent obstacles the dislocation will take the form of a circular arc of dimensionless radius  $R^* (= 1/2 \tau^*)$ . If the distance between any two adjacent obstacles along  $(i)$  exceeds  $2R^*$  or if the dislocation line anywhere intersects itself then the configuration  $(i)$  is transparent to the dislocation and will be by-passed mechanically. If  $(i)$  is not transparent its mechanical stability is governed by the strength of the dislocation-obstacle interaction.

The obstacles are modelled as identical barriers to the dislocation whose effective range of interaction ( $d$ ) is small compared to their mean separation ( $l_s$ ). They may hence be treated as point obstacles. At the  $k^{\text{th}}$  obstacle on  $i$  the dislocation line forms the asymptotic angle  $\psi_1^k$  ( $0 \leq \psi_1^k \leq \pi$ ). The force,  $F_1^k$ , that the dislocation exerts on the  $k^{\text{th}}$  obstacle may be written in dimensionless form

$$\beta_1^k = F_1^k / 2\Gamma = \cos\left(\frac{1}{2}\psi_1^k\right) \quad (3)$$

The dislocation-obstacle interaction is governed by a force-displacement relation <sup>(7)</sup>  $\beta(x/d)$ , the effective dimensionless point force on the

dislocation as it sweeps through (or folds around<sup>(8)</sup>) the obstacle. The maximum,  $\beta_c$ , of this function measures the mechanical strength of the obstacle. A non-transparent line configuration of obstacles constitutes a mechanically stable barrier to the glide of a dislocation under stress ( $\tau^*$ ) if  $\beta_i^k < \beta_c$  for all obstacles  $k$  on  $i$ , hence if  $\beta_i < \beta_c$ , where  $\beta_i$  is the maximum of the  $\beta_i^k$ . The smallest stress  $\tau^*$  at which  $\beta_i > \beta_c$  for all configurations within the array (i.e.,  $\beta_1 > \beta_c$  where  $\beta_1$  is the minimum of  $\beta_i$ ) is the critical resolved shear stress  $\tau_c^*$ . When  $\tau^* < \tau_c^*$  the dislocation will encounter at least one stable configuration within the array, and can glide only with the help of thermal activation.

To phrase a particular case for the present study we chose an obstacle strength  $\beta_c = 0.6$ , which theoretical work by Bacon, Kocks, and Scattergood<sup>(8)</sup> suggests will approximate the effective strength of an "impenetrable" particle in the glide plane. The force-displacement relation,  $\beta(x/d)$ , for such a particle depends on details of the interaction; for simplicity we choose an interaction of simple step form:  $\beta = \beta_c$  when  $0 \leq x/d \leq 1$ ;  $\beta = 0$  otherwise.

If configuration  $i$  is mechanically stable it must be passed by thermal activation. We ignore the possibility of thermally activated bow-out between obstacles and require that activation occur at a particular obstacle. The energetic barrier to thermal activation at the  $k^{\text{th}}$  obstacle on  $i$  is

$$(\Delta G^*)_i^k / kT = \alpha(\beta_c - \beta_i^k) \quad (4)$$

where  $\alpha$  is the dimensionless reciprocal temperature

$$\alpha = 1/T^* = 2\Gamma d / kT \quad (5)$$

The residence time of the dislocation in configuration  $i$  is the time required for thermal activation past at least one obstacle point in  $i$ . The expected value of the residence time is<sup>(5)</sup>

$$\langle t_i^* \rangle = \Lambda_i^{-1} \quad (6)$$

where  $t^*$  is dimensionless time  $\nu t$ ,  $\nu$  is the mean frequency with which the dislocation attempts an obstacle (assumed constant), and  $\Lambda_i$  is the activation parameter

$$\Lambda_i = \sum_{k=1}^{N_i} \exp[-\alpha(\beta_c - \beta_i^k)] \quad (7)$$

where the summation is taken over the  $N_i$  obstacles on  $i$ . The probability that activation will occur first at obstacle  $k$  on  $i$  is

$$\eta(k,i) = \Lambda_i^{-1} \exp[-\alpha(\beta_c - \beta_i^k)] \quad (8)$$

In thermally activated glide the dislocation encounters a sequence of obstacle configurations as it moves through the array (Figure 2). These define the "glide path" ( $\chi$ ) of the dislocation. To compute the glide velocity, we assume that the glide is controlled by thermal activation in the sense that the time required for glide between successive stable configurations along  $\chi$  is negligible compared to the time required for thermal activation past these configurations. If there are  $r$  stable configurations along a particular path  $\chi$  through the array then the expected transit time of a dislocation along  $\chi$  is

$$\langle t_\chi^* \rangle = \sum_{i=1}^r \Lambda_i^{-1} \quad (9)$$

Given that the dislocation may take any one of many available glide

paths through the array the expected transit time is

$$\langle t^* \rangle = \sum_{\chi} \mu_{\chi} \langle t_{\chi}^* \rangle \quad (10)$$

where  $\mu_{\chi}$  is the probability that the path  $\chi$  is followed in a given trial. The velocity of glide is defined in a statistical sense only, but has the ergodic average

$$\langle v^* \rangle = n^{1/2} / \langle t^* \rangle \quad (11)$$

where  $\langle v^* \rangle$  is the dimensionless area swept out by the dislocation per unit time divided by its projected length, the edge length of the array.

The determination of the velocity of glide through a random array of point obstacles is complicated since the available glide paths change with the applied stress and the relative probabilities of these paths change with temperature. The glide path becomes precisely defined only in the limit of very low or very high temperature ( $T^*$ ) or when the applied stress ( $\tau^*$ ) is very close to the critical value ( $\tau_c^*$ ) for athermal glide through the array. When  $T^*$  is small or  $\tau^* \sim \tau_c^*$  the dislocation tends to follow the "minimum-angle" path ( $\chi_0$ ) obtained under the constraint that the dislocation pass each configuration  $i$  by activating past the point  $k$  at which the angle  $\psi_i^k$  takes on its minimum value (or, equivalently, at which  $\beta_i^k$  takes on its maximum value,  $\beta_1$ ). In the limit  $T^* \rightarrow 0$  the velocity is given by the Arrhenius equation

$$\langle v^* \rangle = n^{1/2} \exp[-\alpha(\beta_c - \beta_1)] \quad (12)$$

where  $\beta_1$  is the minimum of the  $\beta_i$ , i.e., the maximum force on the most stable configuration encountered during glide. In the limit  $T^* \rightarrow \infty$  the

glide path becomes a "random" path ( $\chi_R$ ) whose configurations are obtained through a random sequence of activation events. In this case the velocity is again governed by an Arrhenius equation, with pre-exponential and activation energy given by suitable weighted averages over the random configurations. <sup>(5)</sup> At intermediate temperature the equations governing glide are more complex, and cannot easily be set in Arrhenius form.

Given a satisfactory analysis for planes of randomly distributed obstacles one may immediately treat the plastic deformation of an idealized crystal modelled as a stacking of planes of the same type. The model then requires an additional assumption regarding the distribution of dislocations over the glide planes. The simplest assumption, which we shall make in the following, is that each glide plane contains active sources of non-interacting dislocations so that the expected number of dislocations is the same for all planes and all times during steady state deformation. In earlier work <sup>(5)</sup> we termed this a "uniform" distribution of dislocations.

Given a crystal made up of  $S$  parallel glide planes containing a uniform distribution of dislocations the steady state strain rate may be written in the dimensionless form

$$\dot{\gamma}^* = (\rho b / l_s) \bar{v}^* \quad (13)$$

where  $\rho$  is the expected number of dislocations intersecting a dimensionless area perpendicular to the glide planes and  $\bar{v}^*$  is the average of the expected glide velocity for the individual planes in the crystal:

$$\bar{v}^* = \frac{1}{S} \sum_{\ell=1}^S \langle v_{\ell}^* \rangle \quad (14)$$

with  $\langle v_l^* \rangle$  the expected value for the glide velocity of the  $l^{\text{th}}$  plane.

If the individual glide planes contain a finite number of obstacles, then there may be appreciable scatter in the expected glide velocity from one plane to another. This will be reflected in an inhomogeneity of the crystal deformation, which will tend to concentrate on those planes over which glide is easiest ( $\langle v^* \rangle$  is largest). As we shall show below, this plane-to-plane variation in glide velocity becomes less pronounced as the temperature ( $T^*$ ) is increased or as the stress ( $\tau^*$ ) is decreased. Hence crystal deformation becomes more uniform as stress is lowered at constant temperature or as temperature is raised at constant stress.

### III. SIMULATION PROCEDURES

In the work reported here we considered a crystal made up of ten parallel glide planes each of which contained an expected number ( $10^3$ ) of obstacles in a Poisson distribution. The strength of the obstacles was fixed at  $\beta_c = 0.6$  and the force-displacement relation was assumed to have the simple step form described above. The dislocations were assumed uniformly distributed over the glide planes. Hence the dislocation density ( $\rho$ ) in equation (13) could be treated as an arbitrary constant and the steady state strain rate  $\dot{\gamma}^*$  measured by the velocity  $v^*$ . The simulation problem was hence reduced to the problem of computing  $v^*$  as a function of temperature and stress.

To determine  $v^*$  we found the expected glide velocity  $\langle v^* \rangle$  for each of the ten planes as a function of temperature and stress, and summed according to equation (14). The glide velocities were found through direct computer simulation. The simulation code employed is a modification<sup>(9)</sup> of that described in Reference 4. Its procedure is essentially as follows.

Using a pseudo-random number generator the code first fills the area of a square of size  $n$  ( $10^3$  in this case) with a random distribution of points of density one. The array is assumed periodic across all boundaries. The code then introduces a dislocation across the lower boundary of the array and allows it to move forward until it contacts points of the array. The dislocation bows out between adjacent points in a circle of continuously changing radius. The bow-out is terminated by one of three limits. First, the dislocation segment may bow out to the equilibrium radius  $R^*$  without contacting any third obstacle or violating the conditions of mechanical equilibrium ( $\psi > \psi_c$ ) at either of the adjacent obstacles. In this case the dislocation segment is recognized to be mechanically stable. Second, the dislocation may bow to the extent that it violates the condition  $\psi > \psi_c$  at one of the adjacent obstacles. In this case the dislocation is allowed to pass the obstacle, a new segment is defined by the obstacles adjacent to the bypassed obstacle and the bow-out process begun anew. Third, the dislocation may contact a third obstacle during bow-out. In this case the segment is divided, and the stability of the new segments tested by allowing them to bow out in turn. This process of bowing the dislocation between obstacles, defining new segments when obstacles are contacted, and passing obstacles when  $\psi$  falls below  $\psi_c$  is continued until a dislocation configuration is found in which all obstacles are connected by segments which have the equilibrium radius  $R^*$  and the angles at all obstacles are greater than the critical angle  $\psi_c$ . The dislocation is finally tested for self-intersections, which, given the method of construction, must occur at some point other than at an obstacle. If there are

self-intersections, the dislocation is joined at the point of intersection, and a new search is begun. If there are no intersections, the configuration is recognized to be mechanically stable.

Given a stable configuration, the code computes the angles  $\psi_i^k$  along it, and uses the assigned value of the thermal parameter,  $\alpha$ , to compute the mean residence time according to equation (6). It then calls a random number and chooses an activation site according to the probability assignment given in equation (8). The chosen point is passed, and the code then initiates a new search to establish the next stable configuration. In this way a statistically chosen glide path is generated and a transit time is computed according to equation (9). By allowing several sequential passages the ergodic average of the transit time is estimated (equation 10) and the glide velocity  $\langle v^* \rangle$  found.

In simulating deformation of a crystal in which several glide planes must be treated simultaneously over a range of stress and temperature it is tedious and expensive to carry out a full statistical computation of  $\langle v^* \rangle$ . In Reference 5 we identified approximate techniques which appeared particularly promising for use at low temperature. In Reference 4 these were specifically studied. The most promising was the minimal sequence approximation, which ignores the change in glide path with temperature and assumes that the glide path is reasonably approximated by the "minimum angle" path,  $\chi_0$ . This assumption greatly simplifies the computational effort necessary in simulating glide. Since the path  $\chi_0$  is fixed by stress<sup>(4)</sup> a single computer simulation experiment at a given value of  $\tau^*$  yields sufficient information to determine the glide velocity for glide along  $\chi_0$  through a particular array at any value of the temperature.

When the obstacle strength is large, as in the present case, the minimal sequence approximation yields a good estimate for the glide velocity over a large range of temperature. In Figure 3 we compare glide velocity computed in the minimal sequence approximation to that obtained from stochastic treatment of thermal activation for the stress  $\tau^* = 0.4$ . As is apparent from the figure, the approximation yields a reasonable result for values of the thermal parameter ( $\alpha$ ) as low as 10, which corresponds to the lowest realistic value of  $\alpha$  for a deformable metal (Cd at its melting point). We hence employed the minimal sequence approximation to simplify the simulation of crystal deformation.

#### IV. SIMULATION RESULTS

Figure 4 illustrates the central results obtained from simulation of the deformation of an idealized crystal made up of ten parallel glide planes having area  $10^3$ , a uniform distribution of non-interacting dislocations, and a Poisson distribution of obstacles having strength  $\beta_c = 0.6$  and an interaction function,  $\beta(x/d)$ , of simple step form. The figure shows the glide velocity (plotted as  $-\ln v^*$ ) as a function of  $\alpha (=1/T^*)$  for four values of the applied stress,  $\tau^*$ . The light curves show the data for each of the individual glide planes making up the crystal (taken in the minimal sequence approximation); the heavy line gives the resulting deformational velocity ( $\bar{v}^*$ ) for the crystal as a whole.

The glide velocities for the individual planes vary over a range which increases as the temperature is lowered or the stress is raised. The source of this scatter is straight-forward, as may be easily seen from the expression for the glide velocity in the low temperature limit:

$$\langle v^* \rangle = n^{1/2} \exp[-\alpha(\beta_c - \beta_1)] .$$

When the reciprocal temperature  $\alpha$  is large, the velocity is quite sensitive to small plane-to-plane variations in the value of  $\beta_1$ , the maximum force exerted on the most stable configuration encountered in glide along the minimum angle path. We illustrated that variation in Reference 4. In a finite array the variation is significant, and tends to increase with the stress  $\tau^*$ . As temperature is raised the properties of the most stable configuration become less dominant. In the high temperature limit the glide velocity is determined by an average over the forces. Unless  $\tau^*$  is so near  $\tau_c^*$  that there are only a few stable configurations in the array this average tends to be independent of the specific array, and the variation of  $\langle v^* \rangle$  becomes very small.

The consequences of the plane-to-plane variation in glide velocity are illustrated in Figure 5, where we show the appearance of a hypothetical tensile bar made of our model crystal and strained 20% in tension at each of two resolved shear stresses,  $\tau^* = 0.01$  and  $\tau^* = 0.4$ , at temperatures  $T^* = 10^{-3}$ ,  $10^{-2}$ , and  $10^{-1}$ . At low stress ( $\tau^* = 0.01$ ) the deformation is markedly inhomogeneous at the lowest temperature ( $T^* = 10^{-3}$ ), but rapidly becomes homogeneous as temperature is raised. At high stress ( $\tau^* = 0.4$ ) the deformation remains inhomogeneous even at  $T^* = 10^{-1}$ , which roughly corresponds to the highest dimensionless temperature attainable in a typical metal.

The second salient qualitative feature of the data represented in Figure 4 concerns the possibility of representing the deformational velocity by an Arrhenius equation. As  $T^* \rightarrow 0$  the velocity  $\dot{\gamma}^*$  is given precisely by an Arrhenius equation of the form

$$\dot{\nu}^* = \left(\frac{1}{S}\right) \exp[-\alpha(\beta_c - \beta_{1m})] \quad (15)$$

where  $\beta_{1m}$  is the largest of the  $\beta_1$  values for the S planes composing the crystal. However, as  $T^*$  is increased ( $\alpha$  decreased)  $\dot{\nu}^*$  deviates from equation (15) by an amount which represents a balance between the increasing contribution of glide on secondary planes and the increasing importance of secondary activation events in the primary glide plane. As discussed in Reference 5, at intermediate temperature  $\dot{\nu}^*$  tends to fall below the values predicted by the asymptotic relation (15), a result reflected in the slight upward concavity of the curves at  $\tau^* = 0.01-0.25$ . However, as  $\tau^*$  approaches  $\tau_c^*$  this effect is reversed<sup>(4)</sup> and  $\dot{\nu}^*$  tends to exceed the value predicted by equation (15); thus the slight downward concavity of the curve for  $\tau^* = 0.4$ . Note, however, that the data shown here span many orders of magnitude of  $\dot{\nu}^*$ . Were we to confine the data to a range (5-10 orders of magnitude of  $\dot{\gamma}$ ) which might be experimentally measurable, the data would be well fit by an Arrhenius equation at intermediate temperature.

At very high values of  $T^*$  (above the melting point of a plausible crystal in this specific example) a pronounced downward concavity is observed, as shown in the data exhibited in Figure 3. This phenomenon reflects the rapid increase in  $\dot{\nu}^*$  as the probable glide path of the dislocation changes from one dominated by the minimum angle path,  $\chi_0$ , to the much easier glide paths which approach the random path,  $\chi_R$ . The effect is a rapid thermal "softening" of the crystal, which has its source entirely in the thermal choice of glide path; the properties and distribution of obstacles remains the same.

Figure 6 illustrates the variation of glide velocity with stress in tests conducted at constant temperature. In keeping with the conventional representation,

$$\dot{\gamma} = \tau^n \quad (16)$$

the data are plotted in logarithmic coordinates. The stress exponent  $n$  is then the slope of the curve. As is apparent from Figure 6 the data do not show a well-defined stress exponent. The parameter  $n$  is a function of both  $\tau^*$  and  $T^*$ . However, again the data span many orders of magnitude of strain rate; were the data confined to a plausible experimental range a reasonably constant stress exponent would be obtained.

At low temperature ( $T^* = 10^{-3}$ ) the value of  $n$  is large and increases rapidly with stress, from a value of the order of 80 at  $\tau^* = 0.01$  to a value above 300 at  $\tau^* = 0.4$ . As temperature increases both the stress exponent and its stress variation diminish. At  $T^* = 10^{-2}$  the stress exponent is  $\sim 10$  at low stress, increasing to  $\sim 35$  as stress approaches  $\tau_c^*$ . At  $T^* = 10^{-1}$  the stress exponent is near 1.0 at low stress, increasing to about 10 near  $\tau_c^*$ .

The variation of slip morphology with stress at constant temperature is illustrated in Figure 7, where we have shown idealized tensile bars after a strain of 20% at four values of stress ( $\tau^* = 0.01$  to  $\tau^* = 0.4$ ) at  $T^* = 10^{-2}$ . The tendency of the slip to become more inhomogeneous as stress is raised is apparent in the figure.

Finally, we consider the variation of the flow stress (the value of  $\tau^*$  necessary to sustain a constant strain rate, measured by  $\dot{\gamma}^*$  in this model) with the testing temperature. The result depends on the precise

value of  $\dot{\nu}^*$  chosen; when  $T^* > 0$  the flow stress is an increasing function of strain rate. Plots for two choices of  $\dot{\nu}^*$  are shown in Figure 8. The flow stress decreases monotonically from the value  $\tau_c^*$  when  $T^* = 0$ . As expected, the rate of decrease falls as the strain rate is raised. Since in this simple example there is no athermal component to the flow stress, the flow stress asymptotically approaches zero as  $T^*$  approaches infinity for all finite values of  $\dot{\nu}^*$ .

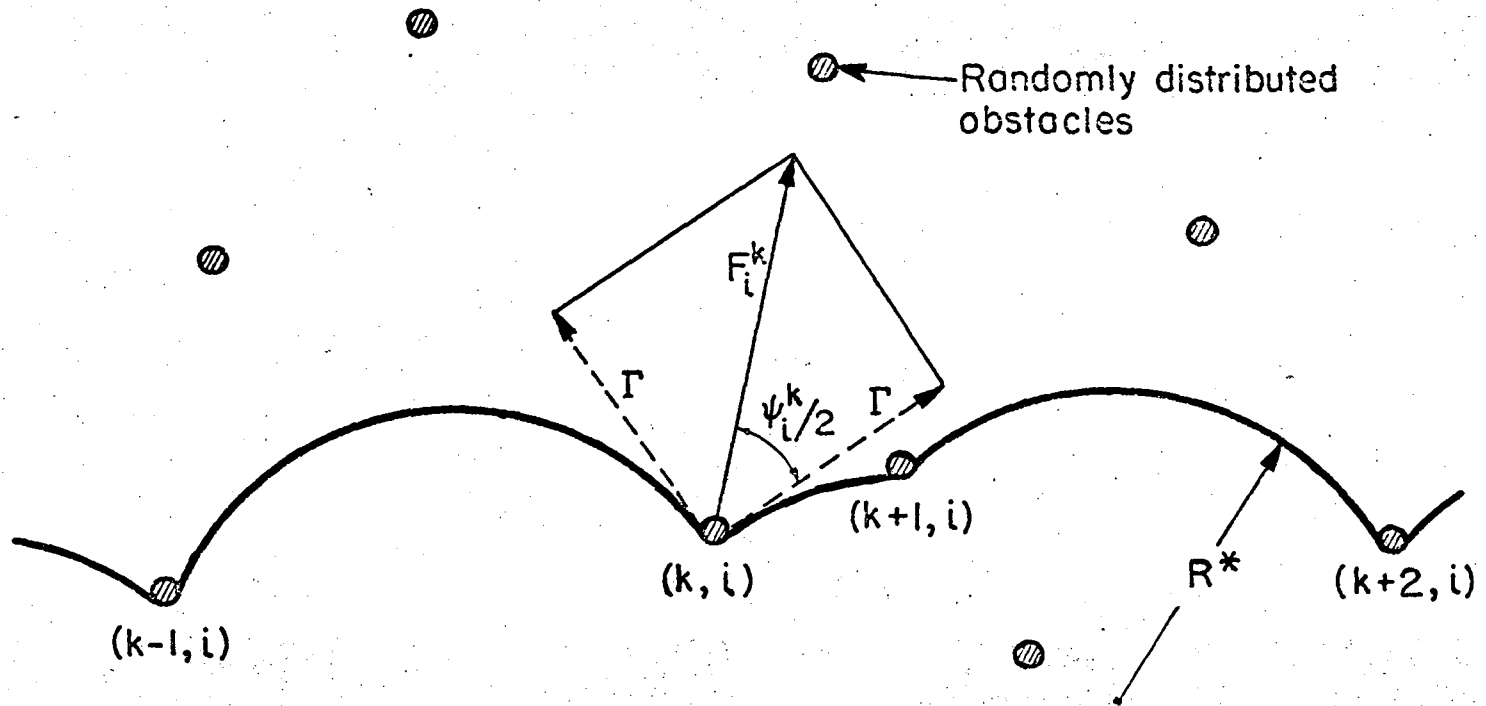
The change in slip morphology with temperature at constant strain rate ( $\dot{\nu}^*$ ) is illustrated in Figure 9. The results qualitatively reproduce those reported in Reference 4. Deformation rapidly becomes homogeneous as  $T^*$  is raised, since both the increase in temperature and the decrease in flow stress favor homogeneous slip.

#### ACKNOWLEDGMENT

This work was supported by the Atomic Energy Commission through the Inorganic Materials Research Division of the Lawrence Berkeley Laboratory.

REFERENCES

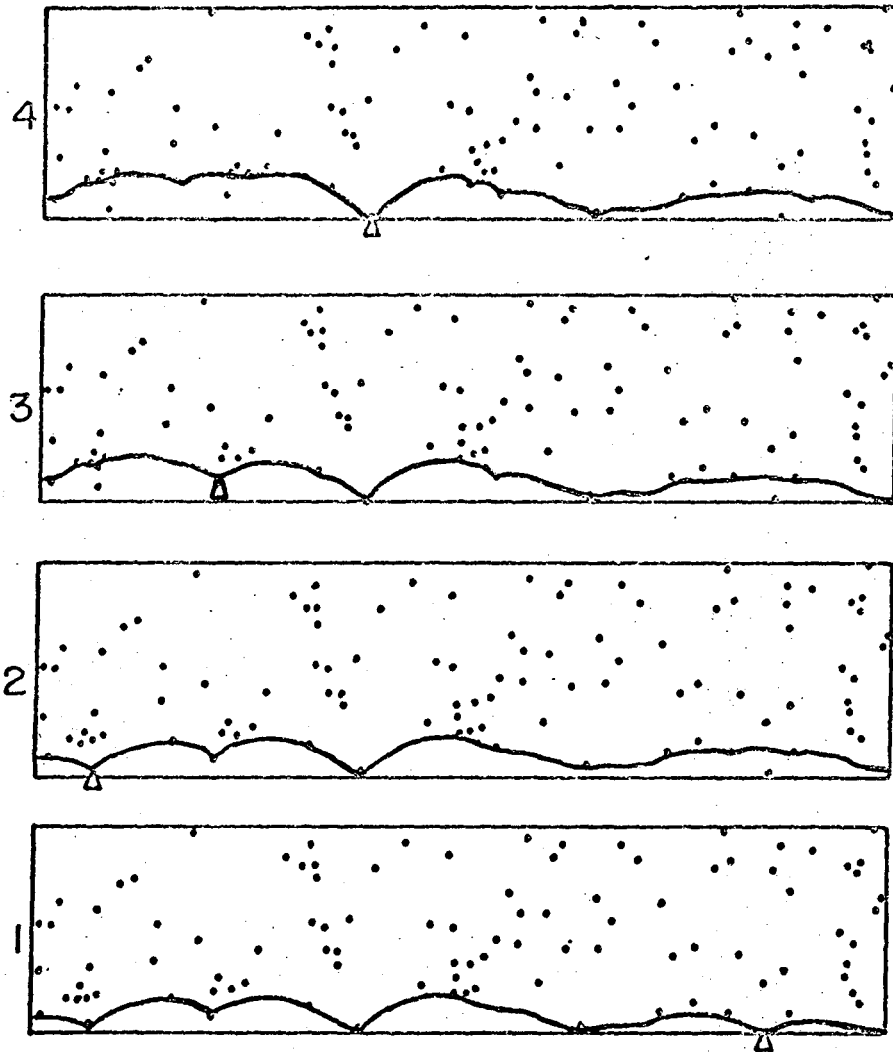
1. J. Friedel, in Electron Microscopy and Strength of Crystals, G. Thomas and J. Washburn, eds. (J. Wiley, New York, 1963), p. 605.
2. A. J. E. Foreman and M. J. Makin, *Phil. Mag.* 14, 911 (1966).
3. D. Klahn, D. Austin, A. Mukherjee and J. E. Dorn, in Advances in Applied Probability, Supplement 2, p. 112 (1973).
4. J. W. Morris, Jr. and Dale H. Klahn, *J. Appl. Phys.* 45, 2027 (1974).
5. J. W. Morris, Jr. and Dale H. Klahn, *J. Appl. Phys.* 44, 4882 (1973).
6. D. H. Klahn and J. W. Morris, Jr., in Rate Processes in Plastic Deformation, J. C. M. Li, ed., Plenum Press (in press).
7. J. W. Morris, Jr. and C. K. Syn, *J. Appl. Phys.* 45, 961 (1974).
8. D. J. Bacon, U. F. Kocks, and R. O. Scattergood, *Phil. Mag.* 28, 1241 (1973).
9. Kenton Hanson, Ph.D. Thesis research (unpublished).



XBL732-5721

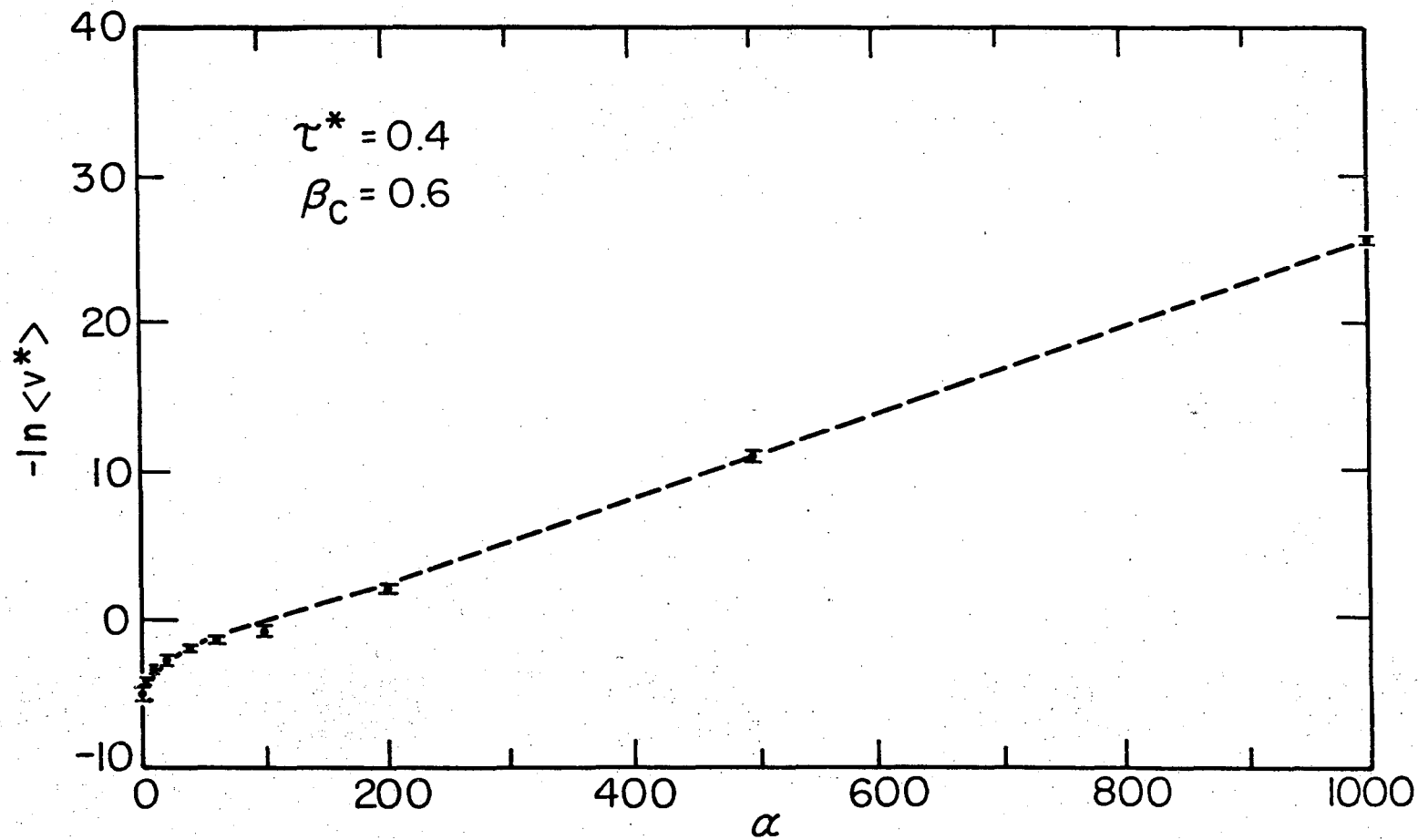
Fig. 1. Configuration of a dislocation pressed against an array of obstacles by a stress  $\tau$ .

00004206737



XBL732-5722

Fig. 2. Sequence of four possible configurations as a dislocation glides into a random array of point obstacles. The activation side is indicated by the symbol ( $\Delta$ ).



XBL 7410-7504

Fig. 3. Comparison of the results using minimum angle approximation (dashed line) and statistically chosen path. The data bars indicated results of four independent trails.

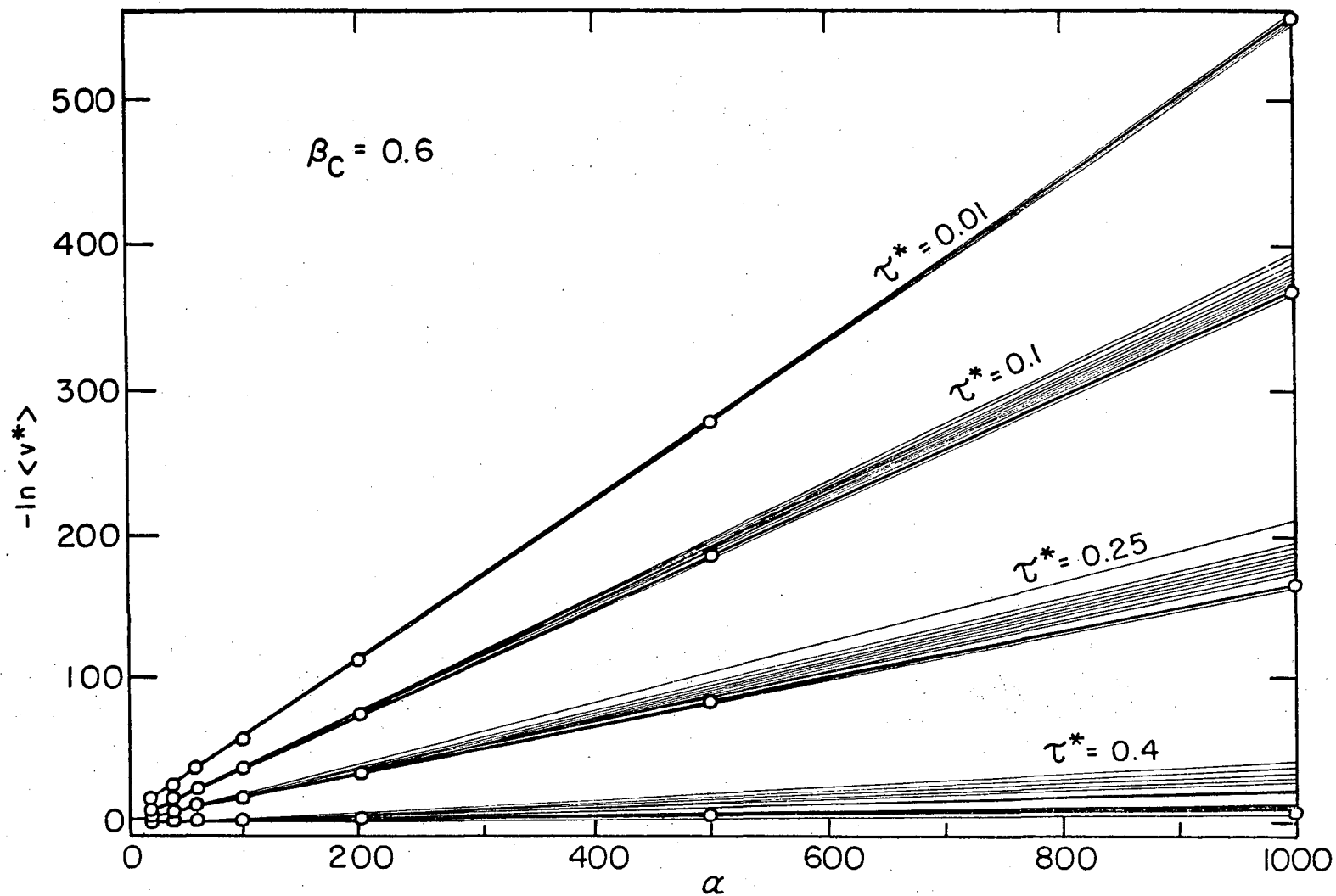


Fig. 4. Comparison of the velocity-temperature relations for ten arrays of  $10^3$  obstacles having  $\beta_c = 0.6$  at each of four stresses (light lines). Also included are the velocity-temperature curves for a crystal made up of these ten arrays under the assumption of a "uniform" distribution of dislocations over the planes (circles, heavy lines).

XBL7410-7520

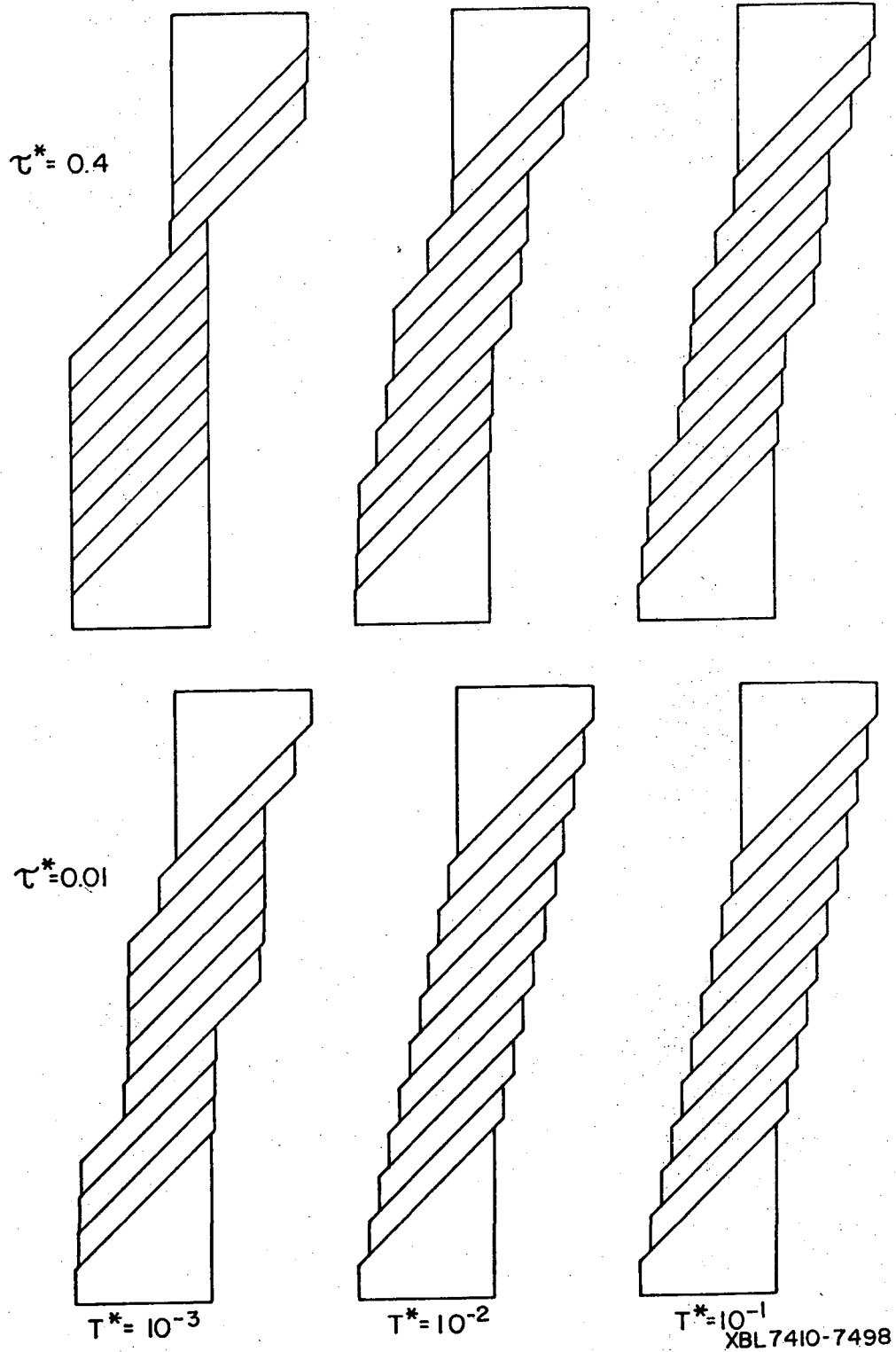
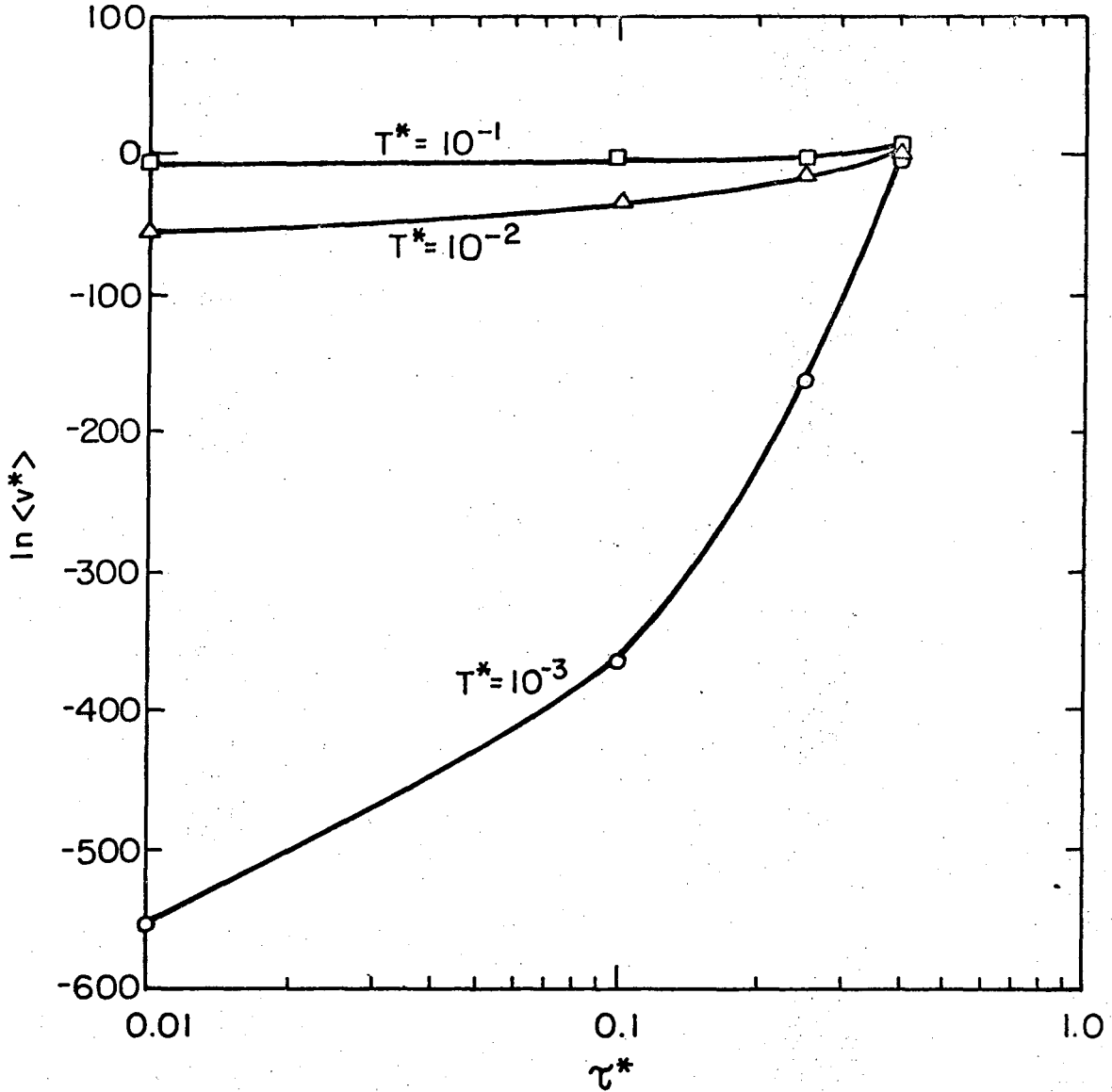
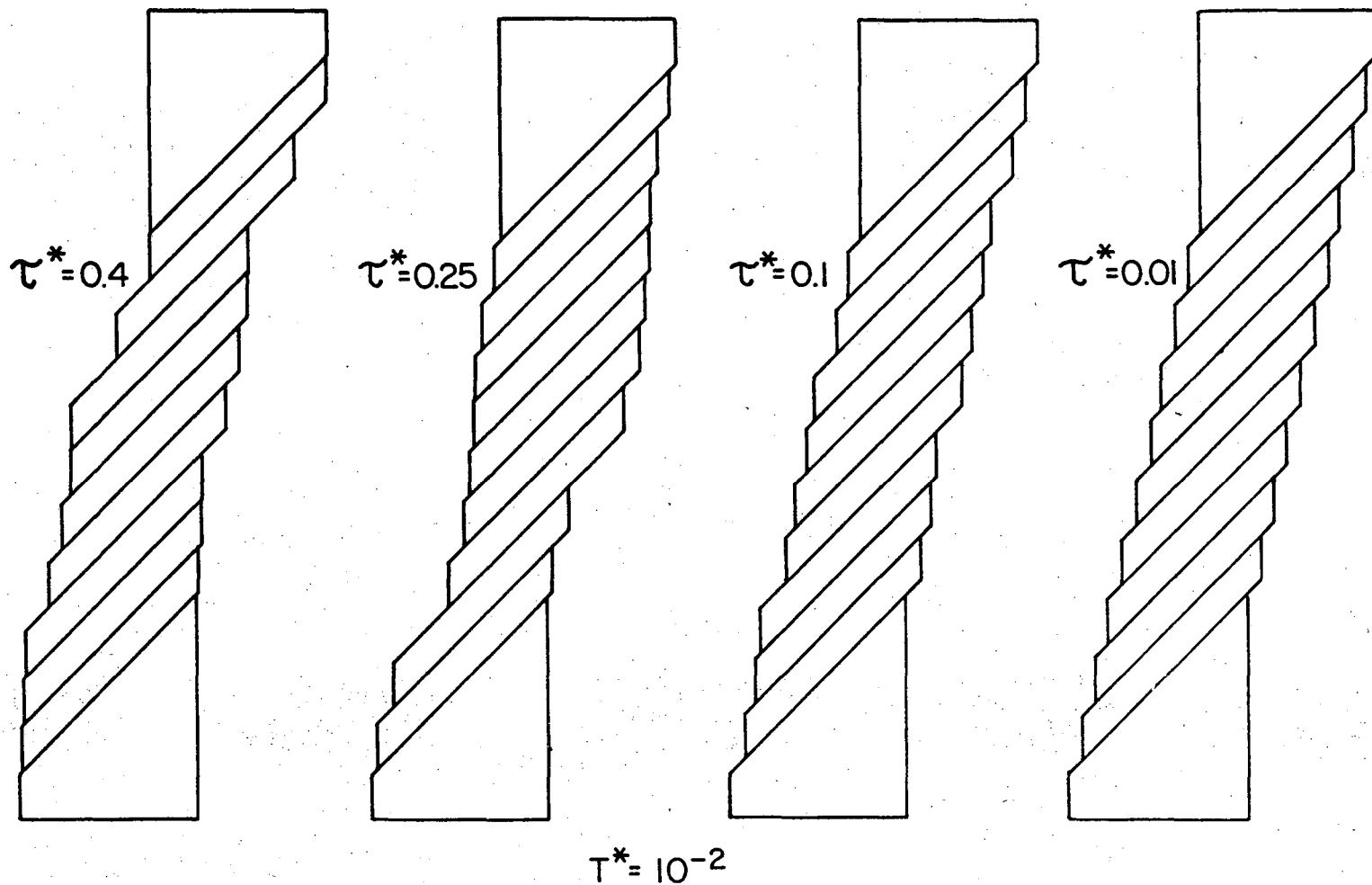


Fig. 5. Illustration of the deformation of a hypothetical crystal made up of ten glide planes whose properties are shown in Fig. 4. This figure shows the change in the appearance of the deformed crystal with temperature, assuming that the crystal contains a uniform distribution of dislocations of fixed density, and is given a total shear strain  $\gamma = 20\%$ .



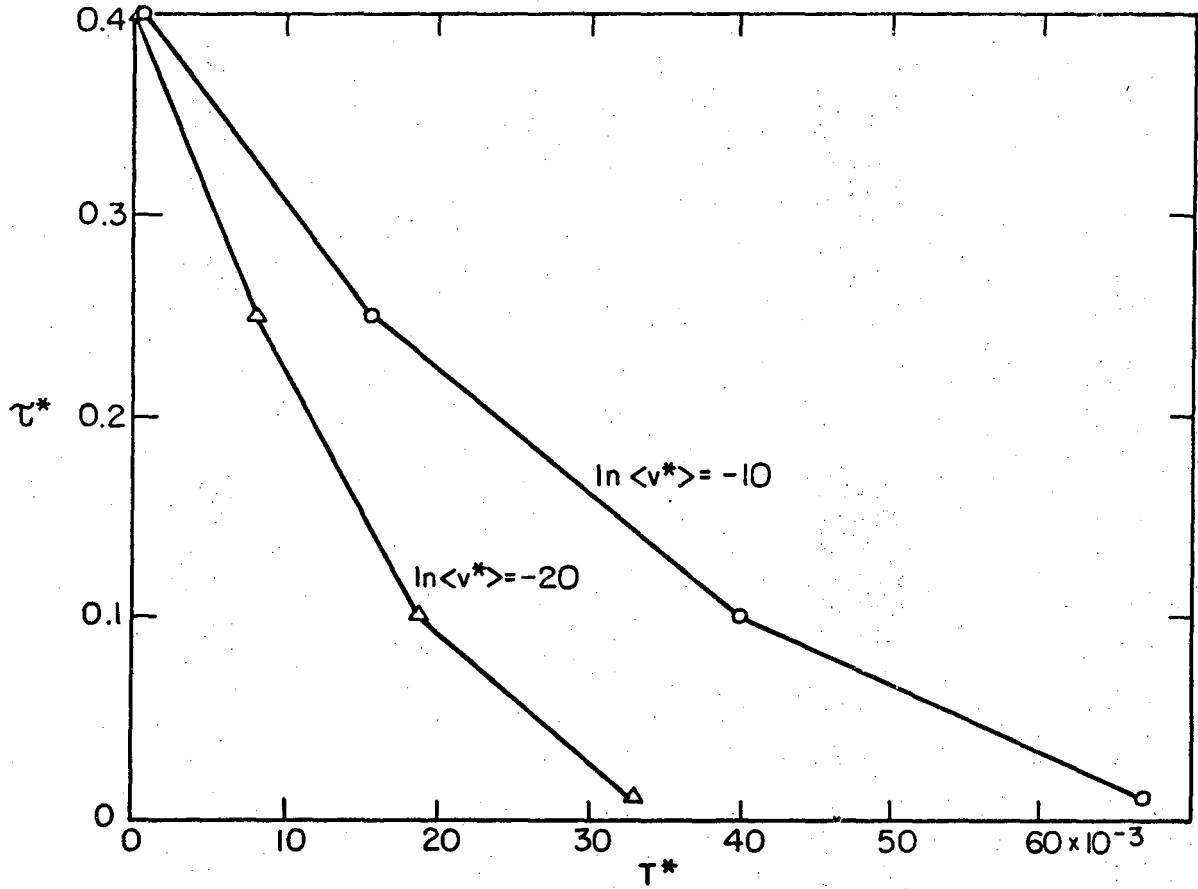
XBL 7410-7502

Fig. 6. Illustration of the variation of glide velocity with stress in tests conducted at constant temperature. In this figure  $\ln \langle v^* \rangle$  is plotted against  $\log \tau^*$  at constant temperature ( $T^* = 10^{-3}, 10^{-2}, 10^{-1}$ ).



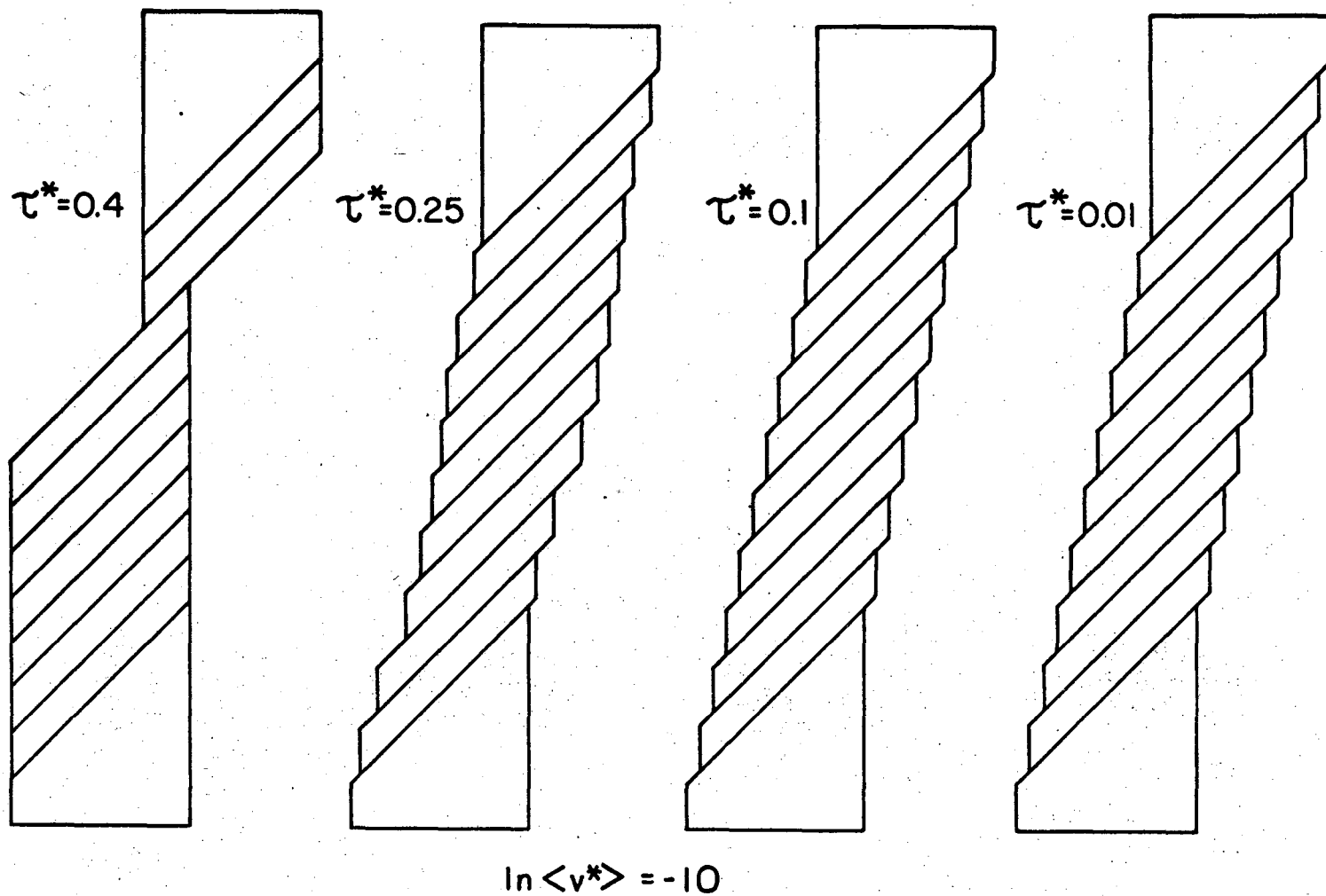
XBL 7410-7500

Fig. 7. Variation of slip morphology with stress at constant temperature. Idealized tensile bars are shown after a strain of 20% at four values of stress ( $\tau^* = 0.01, 0.1, 0.25, 0.4$ ) at  $T^* = 10^{-2}$ .



XBL7410-7521

Fig. 8. The variation of the flow stress with the testing temperature at constant strain rates ( $\ln \langle \dot{v}^* \rangle = -10, -20$ ).



XBL7410-7499

Fig. 9. Illustration of slip morphology with temperature at constant strain rate ( $\ln \langle \dot{\gamma}^* \rangle = -10$ ).

## LEGAL NOTICE

*This report was prepared as an account of work sponsored by the United States Government. Neither the United States nor the United States Atomic Energy Commission, nor any of their employees, nor any of their contractors, subcontractors, or their employees, makes any warranty, express or implied, or assumes any legal liability or responsibility for the accuracy, completeness or usefulness of any information, apparatus, product or process disclosed, or represents that its use would not infringe privately owned rights.*

TECHNICAL INFORMATION DIVISION  
LAWRENCE BERKELEY LABORATORY  
UNIVERSITY OF CALIFORNIA  
BERKELEY, CALIFORNIA 94720